CrystEngComm

Electric-field assisted nucleation processes of croconic acid films

Journal:	*CrystEngComm*
Manuscript ID	CE-ART-09-2019-001493.R1
Article Type:	Paper
Date Submitted by the Author:	20-Oct-2019
Complete List of Authors:	Yuan, Yifan; University of Nebraska-Lincoln, Mechanical and Materials Engineering Department Jiang, Xuanyuan; University of Nebraska - Lincoln, Physics and Astronomy Poddar, Shashi ; University of Nebraska - Lincoln, Physics and Astronomy Xu, Xiaoshan; University of Nebraska-Lincoln, Physics and Astronomy

ARTICLE

Electric-field assisted nucleation processes of croconic acid films

Yifan Yuan,[a] Xuanyuan Jiang,[b] Shashi Poddar [b] and Xiaoshan Xu *[b]

Received 00th January 20xx,
Accepted 00th January 20xx

DOI: 10.1039/x0xx00000x

Growth of organic thin films using physical vapor deposition typically follows a three-dimensional mode, resulting in a rough surface, which undermines their application potentials. To address this issue, we have studied the effect of electric field and temperature on the growth dynamics, especially the heterogeneous nucleation process, of croconic acid (CA) films, taking advantage of the large dipole of the molecules and the ferroelectric polarization of the molecular crystals. We found that the nucleation rate has a maximum at intermediate temperature, and the electric field shifts the maximum nucleation rate towards the lower temperature. An analysis using classical nucleation theory suggests that the electric field decreases sublimation temperature, increases the wetting angle, and decreases the surface diffusion barrier. These results provide important insight into the growth of molecular crystal films under electric fields and pave a way to fabricate films with better surface characteristics for molecular ferroelectric films.

Introduction

Croconic acid ($C_5H_2O_5$ or CA) as a single-component organic ferroelectric compound that exhibits a large spontaneous ferroelectric polarization[1], is a promising candidate to substitute or supplement inorganic ferroelectrics for future electronic and optoelectronic devices, with advantages of light weight, flexibility, and environment-friendly characteristics. The application potential of ferroelectric CA depends on the possibility of fabricating films of well-defined morphology and electric polarization. Various material-processing techniques, such as spin coating[2], matrix-assisted pulsed laser evaporation[3], inkjet printing[4], and physical vapor deposition (PVD), have been employed to prepare CA films. Thermal evaporation as one type of PVD has the advantages of precise thickness control, possibility for ultrathin organic film, and free from contamination. However, two fundamental issues still need to be addressed. First, due to the weak interaction at the organic/inorganic interface, the growth of organic films on inorganic substrates tend to adopt an island-formation mode[5], resulting in a rough surface[6,7], which affect the device performance.[8] For instance, the carrier mobility and On/Off ratio were significantly reduced with the film roughness in organic thin film transistor.[9] Second, non-epitaxial growth typically leads to polycrystalline films, which undermines the net electric polarization. Our previous work[7] indicated that the remnant polarization in the polycrystalline films was much lower than that of single crystals.

Here we attack the problem using physical vapor deposition assisted by an electric field. The dipole moment carried by the CA molecules and the spontaneous polarization of the CA crystals offer an additional knob in controlling the film growth and aligning the molecular dipoles by varying the energetics of the growth. An electric field E may contribute to the electrostatic energy of a dipole D by ED. For CA (D=2.5018×10^{-29} Cm)[10] in an electric filed 2 MV/m, which is lab-achievable, the electrostatic energy is equivalent to the thermal energy at temperature about 4 K. On the first look, this energy is not expected to generate a large impact on film growth unless at very low temperature. However, this estimation is based on fully equilibrium state of the film/substrate. In fact, the film growth on a substrate involves a sequence of inequilibrium processes, such as deposition, surface diffusion, and desorption, followed by nucleation and post-nucleation growth[11,12], as illustrated in Fig. 1. [13] In particular, from the classical nucleation theories (CNT), the dynamic nucleation process is governed by competition between the volume enthalpy change, surface, and interfacial energies[14], which leads to its strong temperature dependence. It is possible that an electric field may impact this dynamic process, especially when the electrostatic energy of the dipoles can tip the balance in a close energy competition. Indeed, previous experiments validated that the external electric field promoted nucleation in different systems.[15] For instance, the electric field produced nucleation of bubbles at lower superheat ΔT (temperature of the liquid minus the boiling point) of organic liquids.[16] He et al.'s experimental research indicated that the external electric field largely increased the ion-induced nucleation rate.[17] In terms of nucleation in aqueous medium[18], it is shown that the nucleation rate of NaCl crystal is increased by 233% by an electric field strength of 0.1 MV/m.

[a] Department of Mechanical and Materials Engineering, University of Nebraska, Lincoln, Nebraska, 68588, USA.
[b] Department of Physics and Astronomy, University of Nebraska, Lincoln, Nebraska 68588, USA. E-mail: xiaoshan.xu@unl.edu

In this work, we studied temperature-dependent CA film growth in a 2.1 MV/m out-of-plane electric field, focusing on the nucleation process using a 5 nm nominal thickness to avoid grain coalition. The results confirm the non-monotonic temperature dependence predicted by CNT, where a maximum nucleation rate occurs in the intermediate temperature. The electric field clearly shifts the temperature dependence of the nucleation rate. An analysis in terms of CNT reveals the substantial effects of electric field on the critical gas-solid transition temperature, film/substrate interfacial energy, and surface diffusion energy.

Experimental

Preparation of CA films with and without the electric field

Croconic acid powders from Alfa Aesar, with purity of >98%, were used as the source material. The substrates are 100 nm Au(111)/10 nm Ti(111)/Si(100). Films were deposited in pairs simultaneously, one with and one without electric field, at various temperatures. Their deposition time (42 min) and distance (~50 cm) between the source and the substrate were the same. The configuration for each film is shown in Fig. 2(a), where the conductive meshes (46 μm hole) is separated from the substrate by 100 μm. A voltage bias of 210 V was applied to the mesh of one of the films, corresponding to an electric field 2.1 MV/m. All films were deposited by thermal evaporation using an EvoVac deposition system from Angstrom Engineering with a rate of 0.02 Å/s, an initial pressure 1.3×10^{-4} Pa, and a nominal thickness of 5 nm. The source-substrate distance was 25 cm. The substrate temperature was controlled using a liquid-nitrogen flow cryostat. Before deposition, the substrates were rinsed with isopropanol and deionized water three times. After the deposition, the substrate temperature was warmed up slowly to room temperature before the films were taken out of the growth chamber.

Morphology and structural characterizations

Atomic force microscopy (AFM) images with a resolution of 512×512 pixels and an area of 1 μm^2 were collected by the Bruker Dimension Icon system in a ScanAsyst automatic image optimization mode and analyzed using Gwyddian software. X-ray diffraction (XRD) was carried out using a Bruker D8 Discover diffractometer with the fixed incident angle ω=10° to verify the crystal structure of grown films using a thick (950 nm) film due to the small structural factor of the light elements in croconic acid, as shown in Fig. 2(b). The diffraction peaks of the film, which were normalized to the intensity of (210) plane, matched well with the standard pattern of croconic acid from CCDC nos. 147324[19]. All the measurements were performed at room temperature and ~60% RH within one day after the films were deposited.

Results and Discussion

Morphology of CA film

Fig. 3 shows the AFM images of films grown with and without the electric field at three different temperatures, and the corresponding height histograms $P(z)$ as the insets, where P is probability and z the height. All images have the same color and length scale. The height histogram of each film can be decomposed into the substrate and film peaks at smaller and larger height respectively. The position of the substrate peak is set to zero as the reference.

Overall, the film consists of well-separated CA grains due to the small nominal thickness. The film morphology changes dramatically with temperature, at both low (258 K) and high (283 K) temperature, the coverage of the substrate surface is low, as seen from the intense substrate peak, although at high temperature the CA grains tend to have more facets. In contrast, at intermediate temperature, such as 273 K, a large number of CA grains were found on the substrates, leading to a larger coverage, as seen from the weak substrate peak. When the substrate temperature is increased to 293 K, the number of grains is too small to distinguish CA film from the substrate using an optical microscope. For higher temperatures, no CA grains could be found.

The effect of electric field is also visible from Fig. 3. In particular, at 273 K, the CA grains grown within the electric field has a larger dispersion of height, as indicated by the wider film peak in Fig. 3(d) compared with that in Fig. 3(c). This larger dispersion of height remains at 283 K when the growth is under the electric field, as indicated by the longer tail of the histogram and apparently larger grain size in Fig. 3(f) compared with that in Fig. 3(e). At 283 K, the impact of electric field on the shape of the grains is also discernable: without electric field, the grains are more elongated than those grown with the electric field.

Nucleation process

In the case of low coverage and not so high temperature, the nucleation rate is proportional to the grain density, assuming no coalition of nuclei‡. Therefore, to quantify the effect of temperature and electric field on the nucleation process of CA films, we analyzed the grain density of the films using the height histogram $P(z)$. The grains were identified above a threshold height z_0 which was determined as the intersection point of the substrate peak and the film peak and above which grains were clearly differentiated from the background. Each data point is the average of three AFM measurements on different areas of the same film. Error bars show the standard deviation from the mean.

The grain densities are plotted against temperature with and without electric field in Fig. 4(a) respectively. Regardless of the presence of an electric field, the grain density as a function of temperature shows a maximum. The electric field has a clear effect that shifts the maximum grain density from about 273 K to about 258 K. The largest impact of the electric field occurs at 243 K, where the average grain density changes from 234 to 452 μm^{-2}, corresponding to

93% increase, whereas it decreases from 59.6 to 0 μm^{-2} at 293 K.

The temperature dependence of the nucleation rate has been studied previously[20–22], especially on the steady-state nucleation rate J_0. In case of the heterogeneous nucleation from vapor with a constant impinging rate[23], the nucleation rate is related to the transport barrier E_{tr} and nucleation barrier ΔG^*:

$$J_0(T) = \frac{1}{(kT)^{\frac{1}{2}}}\Gamma \exp\left(-\frac{E_{tr}}{kT}\right)\exp\left(-\frac{\Delta G^*}{kT}\right) \quad (1)$$

$$\Gamma = 2\sigma^{1/2} v_c \frac{\nu l}{v_g^2}(1-\cos\theta) \quad (2)$$

$$\Delta G^* = \Omega \frac{T_m^2}{(\Delta T)^2} \quad (3)$$

$$\Omega = \frac{16\pi\sigma^3 v_c^2 \phi(\theta)}{3\Delta h_m^2} \quad (4)$$

where θ is the wetting angle [Fig. 4(b)], ν is a frequency factor, l is the mean free path of molecules in the gas, $1/v_g$ is the number of gaseous molecules in unit volume, Δh_m is the enthalpy change of sublimation (latent heat), T is the temperature, T_m is the equilibrium gas-solid transition temperature, $\Delta T = T_m - T$, v_c is the molar volume of the crystal phase, σ is the surface energy, $E_{tr} = E_{sd} - E_{des}$, E_{des} is the activation energy for desorption, E_{sd} is the activation energy for surface diffusion, k is Boltzmann constant, and the wetting function is

$$\phi(\theta) = \frac{1}{4}(1-\cos\theta)^2(2+\cos\theta) \quad (5)$$

One can understand the temperature dependence of the nucleation rate $J_0(T)$ from Eq. (1). Since the nucleation barrier $\Delta G^* \propto 1/(\Delta T)^2$, when $T \rightarrow T_m$ ($\Delta T \rightarrow 0$), ΔG^* approaches infinity, corresponding to the diverging barrier around the gas-solid phase transition temperature. Therefore, at high temperatures, increasing temperature decreases nucleation rate; this is the nucleation-barrier-limited region. At low temperatures, the nucleation barrier ΔG^* approaches a constant. The factor $\exp(-\Delta G^*/kT)\exp(-E_{tr}/kT)$ then determines the temperature dependence of the nucleation rate. In other words, at low temperature, the reduced thermal energy reduces the chance of molecules overcoming the diffusion and nucleation barrier, which leads to the diminishing nucleation rate; this is the diffusion-limited region. The different temperature dependences at low and high temperature ranges then result in a maximum nucleation rate at the intermediate temperature, as observed in Fig. 4(a).

To gain quantitative understanding of the nucleation process, i.e. the critical parameters that govern the nucleation rate $J_0(T)$, one may fit the experimental observation in Fig. 4(a) with the classical nucleation theories. The fitting is carried out using Eq. (1) with four fitting parameters Γ, E_{tr}, T_m, and Ω. The fitted curves are plotted in Fig. 4(a) and the fitting parameters are shown in Table 1. To the best of our knowledge, these parameters for CA grown on Au (111) haven't been reported before.

For the barrier coefficient Ω, the fitted value with electric field is larger than that without electric field, as seen in Table 1, implying the increased nucleation barrier by the electric field. At high temperature or nucleation-barrier-limited region, the diffusivity of molecules is large enough. The direct consequence of the increased nucleation barrier by the electric field is the reduced nucleation density at the higher temperature as shown in Fig. 4(a). At 273 K, the electric field increases the nucleation barrier from 0.012 eV to 0.023 eV. To further analyze the reasons for the increased Ω, we examine the relation between the surface energy and the sublimation energy[24],

$$\sigma = k_c\left(\frac{\Delta h_m}{N_A^{1/3} v_c}\right)^{2/3} \quad (6)$$

where N_A is Avogadro's number, k_c is a constant. Substituting Eq. (6) into Eq. (4), one has $\Omega = \frac{16\pi k_c^3}{3N_A^{2/3}}\phi(\theta)$. In other words, the increase of Ω is directly caused by the increase of $\phi(\theta)$, corresponding to the increase of wetting angle θ. If we assume that the nucleus has the shape of a spherical cap, the wetting angle θ is related to the aspect ratio λ_n of the nucleus, whose definition is seen in Fig. 4(b),

$$\cos\theta = (1-4\lambda_n^2)/(1+4\lambda_n^2) \quad (7)$$

The fact that θ increases in the electric field implies that λ_n also increases.

According to the well-known relation of Young[23], $\cos\theta = (\sigma_s - \sigma_i)/\sigma$, the wetting angle θ is the balanced result of free surface energy of nucleus σ and the substrate σ_s, and of the substrate-nucleus interface σ_i [Fig. 4(b)]. It is unlikely that a change in σ_s is the underlying factor for the shift in the wetting angles. Therefore, the large increase of θ could be attributed to the increase of σ_i and σ in the electric field. It was found[6] that the planar CA molecules tend to lie down on the Au substrate with their polar axes in the film plane.[25] As shown in Fig. 4(b), if α is the angle between molecules and the surface, the fact that molecules tend to lie down on the surface implies that σ_i is minimal when α is zero. When there is an out-of-plane electric field, the molecules tend to align their polar axis along the field direction, which means increasing α and σ_i. Therefore, wetting angle θ tends to increase with the out-of-plane electric field according to the relation of Young.[23] Similarly, the wetting angles of some polar droplets, such as alcohols, alkanes, and octanol, increase in the out-of-plane electric field as well which is also attributed to the increase of interface energy σ_i.[26]

For the diffusion barrier E_{tr}, 0.19 eV and 0.14 eV were found from the fit for E=0 and E=2.1 MV/m respectively. These values are comparable with that of H atomic diffusion on the Cu (001) surface (0.197 eV)[27], and water monomer on Pd(111) (0.13 eV)[28], in agreement with the analysis reported by Hooper et al. [25] concerning the diffusion of CA molecules on Au (11) and Ag (111). The reason that the electric field reduces the transport barrier of nucleation may be related to the increase of the interfacial energy σ_i by the

electric field. As discussed above, the out-of-plane electric field tends to pull the molecular polar axis away from the substrate surface and increase σ_i; this leads to a weaker binding between the molecules and the substrate surface and lower diffusion barriers.

For the solid-gas transition temperature T_m, the fit suggests that the value reduces from 303 K to 300 K in the E=2.1 MV/m out-of-plane field. In particular, at 293 K, no CA grains formed on the substrate with the electric field compared with a few grains on films grown without the electric field. Similar results were found earlier regarding the decreased melting temperature of gold in strong electric field.[29] From classical thermodynamics, the change of Gibbs free energy in the phase transformation is $\Delta g = \Delta h - T\Delta s$. At equilibrium transition temperature T_m the free energies of gas and solid are equal, i.e. $\Delta g = 0$. Consequently

$$T_m = \Delta h / \Delta s \quad (8)$$

where $\Delta h = h_{gas} - h_{solid}$, h_{gas} and h_{solid} are the enthalpy of the gas and solid phases respectively. Naturally, one may expect that the electric field would lower h_{solid} since the solid CA consists of aligned electric dipoles which may reduce the energy. However, since the in-plane dipole moments of the CA molecules are mostly perpendicular to the out-of-plane electric field, the contribution of electrostatic energy to the enthalpy in the solid CA is minimized. In contrast, in the gas phase, molecules can be aligned by the electric field and reduce h_{gas}. The reduced h_{gas} leads to decreased T_m.

Thus, the out-of-plane electric field decreases the surface diffusion barrier (E_{tr}) of CA on Au (111), increases the interface energy (σ_i), and increases T_m. These factors cause the shift of temperature profile of the nucleation rate. It is expected that when the system size increases, e.g., when the films are thick enough to cover the whole substrate, the nucleation rate will increase because the underlying CA film instead of Au becomes the effective substrate. Unfortunately, we could not predict the scaling of the electric field's effect with thickness under current model. Generally, the effect of electric field in the phase transformation depends on the nature of the transitions. Radacsi's review[30] demonstrated the positive effect of DC/AC electric field toward crystallization from solution including reducing nucleation time, and orienting crystallites. In terms of nucleation from vapor phase, Ghosh[31] demonstrated the increase of transient nucleation rate of charged droplets in the water vapor. The electric field can also align molecules in the deposition from vapor.[32]

The above analysis uses the intersection point of the substrate peak and the film peak (Fig. 3) to define grains. However, very small particles, e.g., with ~10 nm diameter and ~ 1 nm height in Fig. 3(a), exist as well; they are included in the substrate peak. Their nucleation mechanism is different from the above-discussed process that requires diffusion. Instead, those particles nucleate on the substrate defects, such as step edges, corresponding to much lower nucleation barriers; desorption factor then plays a major role in the process. The diagram for this process is illustrated in Fig. 5(c). The desorption process limits the growth rate according to the factor $\exp(E_{des}/kT)$, which predicts monotonic increase of film thickness or coverage with temperature. This can be seen in Fig. 5(a), where excluding the peaks, the mean thickness increases as temperature decreases.

Post-nucleation growth process

After nucleation, the nuclei continue to grow with influx of molecules and cover the substrate. We obtained coverage as $\int P(z)dz$ ($z_0<z<\infty$) for the film peak. The coverage rate of films is calculated by the projected area of grains divided by the whole area. The largest coverage rate is at 273 K shown in Fig. 5(b). The electric field has no obvious effect on film coverage.

On top of the background of monotonic temperature dependence, there is a peak in the temperature dependence of $\langle z \rangle$ between T = 260 and 285 K [Fig. 5(a)]. Naturally, this can be related to the peak in the temperature dependence of the grain density. On the other hand, the peak position appears to be independent of the electric field, although the peak intensity is clearly enhanced by the electric field. Therefore, the electric field may affect not only the nucleation process (grain density), but also the growth of the crystallites, especially the shape of the grains, as observed by comparing Fig. 3(e) and (f).

To further demonstrate whether the electric filed will facilitate the preferential growth, we define d as the equivalent diameter of a grain's projected area, z_{max} as the maximum height difference of the grain. Both d and z_{max} can be found once the grains are defined using the height threshold. The normal elongation ratio is:

$$\lambda = z_{max}/d \quad (9)$$

The representative histogram of λ for temperature 273 K is shown in Fig. 6(a). The peak of λ is shifted from 0.132 to 0.22 by the electric field, indicating that the electric field indeed accelerated the growth along the out-of-plane direction for the temperature 273 K. The comparison of the mean λ for the electric field condition is plotted against the substrate temperature, as shown in Fig. 6(b). At higher substrate temperature (>270 K) the electric field induced a remarkable normal growth along the electric field direction. However, this kind of "electric" growth is not obvious for the lower temperatures.

The anisotropic growth of CA crystallites after nucleation is in agreement with the previous discussion for the nucleation process, where the electric field increases λ_n by increasing wetting angle θ. To quantitatively analyze its change, we assume that the grains have the shape of a spherical cap. At 283 K, λ is increased from 0.143 to 0.184 by the electric field [Fig. 6(b)], corresponding to θ = 31.8° and 40.5° according to Eq. (7); $\phi(\theta)$ then increases by 2.45 times. On the other hand, from the fitting results in Table. 1, Ω or $\phi(\theta)$ increases by 1.58 times. This agreement is fair considering that the final aspect ratio is also affected by the post-nucleation growth process.

In other words, the observation of the larger electric field effect on $\phi(\theta)$ than that analyzed in the nucleation

process, suggest that the electric field also has a significant impact on the post-nucleation growth process. This effect appears to be larger at higher temperatures, according to Fig. 6(b). At high temperature, the surface diffusion is enhanced by the thermal energy, which promotes post-nucleation growth. Therefore, the apparent larger effect of the electric field on the aspect ratio of the grains at higher temperatures is probably because of the more significant contribution of post-nucleation growth to the grain.

Conclusions

In summary, we have studied the nucleation and growth behavior of croconic acid molecules under different substrate temperatures and the electric field. The heterogeneous nucleation could be described by classical nucleation theory. The mechanisms and parameters responsible for the nucleation rate with and without the electric field were quantitatively analyzed. We show that (1) The electric field shifts the peak position of the maximum nucleation rate toward the lower temperature. This is mainly due to the reduced transport barrier of nucleation from 0.19 eV to 0.14 eV, increased interface energy, and reduced equilibrium transition temperature from 303 K to 300 K by the electric field. (2) The electric field induces the preferred growth along the out-of-plane direction at higher temperatures. The anisotropic growth is consistent with the increased wetting angle of nuclei in the electric field. These results provide insights into the effect of electric field on molecular crystal nucleation and growth on inorganic substrates, which could be utilized to improve the vacuum deposition process of organic films and achieve better surface morphology of organic films.

Conflicts of interest

We declare no conflicts of interest.

Acknowledgements

The authors acknowledge the support from the National Science Foundation through the Materials Research Science and Engineering Center (Grant No. DMR-1420645). The research was performed in part in the Nebraska Nanoscale Facility: National Nanotechnology Coordinated Infrastructure and the Nebraska Center for Materials and Nanoscience (and/or NERCF), which are supported by the National Science Foundation under Award ECCS: 1542182, and the Nebraska Research Initiative.

Notes and references

‡ It is observed that at 293 K, large grains are surrounded by small clusters as Oswald ripening[33], shown in Fig. S1 (Supplementary Information). It only appeared at very high temperature due to sufficiently large diffusion length of molecules.

1 S. Horiuchi, Y. Tokunaga, G. Giovannetti, S. Picozzi, H. Itoh, R. Shimano, R. Kumai and Y. Tokura, *Nature*, 2010, **463**, 789–792.
2 D. B. Hall, P. Underhill and J. M. Torkelson, *Polym. Eng. Sci.*, 1998, **38**, 2039–2045.
3 S. M. O'Malley, S. Y. Yi, R. Jimenez, J. Corgan, J. Borchert, J. Kuchmek, M. R. Papantonakis, R. A. McGill and D. M. Bubb, *Appl. Phys. A Mater. Sci. Process.*, 2011, **105**, 635–641.
4 S. Horiuchi and Y. Tokura, *Nat. Mater.*, 2008, **7**, 357–366.
5 B. F. Usher, *Appl. Surf. Sci.*, 1985, **22–23**, 506–511.
6 L. Hu, R. Feng, J. Wang, Z. Bai, W. Jin, L. Zhang, Q. M. Nie, Z. J. Qiu, P. Tian, C. Cong, L. Zheng and R. Liu, *Adv. Funct. Mater.*, 2018, **28**, 1–9.
7 X. Jiang, H. Lu, Y. Yin, X. Zhang, X. Wang, L. Yu, Z. Ahmadi, P. S. Costa, A. D. Dichiara, X. Cheng, A. Gruverman, A. Enders and X. Xu, *Appl. Phys. Lett.*, 2016, **109**, 102902.
8 X. Liu, Z. Cai, S. Liu, J. Peng and M. Zhu, *Microelectron. Reliab.*, 2017, **74**, 100–109.
9 P. S. Jo, J. Sung, C. Park, E. Kim, D. Y. Ryu, S. Pyo, H. C. Kim and J. M. Hong, *Adv. Funct. Mater.*, 2008, **18**, 1202–1211.
10 S. Horiuchi, Y. Tokunaga, G. Giovannetti, S. Picozzi, H. Itoh, R. Shimano, R. Kumai and Y. Tokura, *Nature*, 2010, **463**, 789–792.
11 A. C. Zettlemoyer, *Nucleation*, Marcel Dekker, New York, 1969.
12 D. A. Porter, K. E. Easterling and M. Y. Sherif, *Phase transformations in metals and alloys*, Routledge, 3rd edn., 2009.
13 H. Guo, D. Sun, W. Wang, Z. Gai, I. Kravchenko, J. Shao, L. Jiang, T. Z. Ward, P. C. Snijders, L. Yin, J. Shen and X. Xu, *J. Appl. Phys.*, 2013, **113**, 234301.
14 T. H. Zhang and X. Y. Liu, *Angew. Chemie - Int. Ed.*, 2009, **48**, 1308–1312.
15 M. Sakai, M. Iizuka, M. Nakamura and K. Kudo, *Jpn. J. Appl. Phys.*, 2004, **43**, 2362–2365.
16 D. S. Parmar and A. K. Jalaluddin, *J. Phys. D. Appl. Phys.*, 1975, **8**, 971–982.
17 F. He and P. K. Hopke, *J. Chem. Phys.*, 1993, **99**, 9972–9978.
18 K. V Saban, J. Thomas and G. Varghese, *Indian J. Phys.*, 2002, **76**, 355–359.
19 D. Braga, L. Maini and F. Grepioni, *CrystEngComm*, 2004, **3**, 27.
20 C. N. Nanev, *Theory of Nucleation*, Elsevier B.V., Second., 2014, vol. 1.
21 P. F. James, *Phys. Chem. Glas.*, 1974, **15**, 95–105.
22 D. Kashchiev, *Nucleation*, Elsevier Science, 2000.
23 I. V Markov, *Crystal Growth For Beginners: Fundamentals Of Nucleation, Crystal Growth And Epitaxy (2nd Edition)*, World Scientific Publishing Company, 2003.
24 D. Tabor, *Gases, liquids and solids: and other states of matter*, Cambridge University Press, 1991.
25 J. Hooper, D. A. Kunkel, E. Zurek and A. Enders, *J. Phys. Chem. C*, 2015, **119**, 26429–26437.
26 A. Bateni, S. Laughton, H. Tavana, S. S. Susnar, A. Amirfazli and A. W. Neumann, *J. Colloid Interface Sci.*, 2005, **283**, 215–222.
27 J. Kua, L. J. Lauhon, W. Ho and W. A. Goddard, *J. Chem. Phys.*, 2001, **115**, 5620–5624.

28 V. A. Ranea, A. Michaelides, R. Ramírez, P. L. De Andres, J. A. Vergés and D. A. King, *Phys. Rev. Lett.*, 2004, **92**, 1–4.
29 L. De Knoop, M. Juhani Kuisma, J. Löfgren, K. Lodewijks, M. Thuvander, P. Erhart, A. Dmitriev and E. Olsson, *Phys. Rev. Mater.*, 2018, **2**, 1–6.
30 L. F. Alexander and N. Radacsi, *CrystEngComm*, 2019, **21**, 5014–5031.
31 M. Ghosh, *RSC Adv.*, 2014, **4**, 45275–45285.
32 T. Mandal, A. Garg and Deepak, *J. Appl. Phys.*, , DOI:10.1063/1.4826212.
33 Z. Zhang, Z. Wang, S. He, C. Wang, M. Jin and Y. Yin, *Chem. Sci.*, 2015, **6**, 5197–5203.

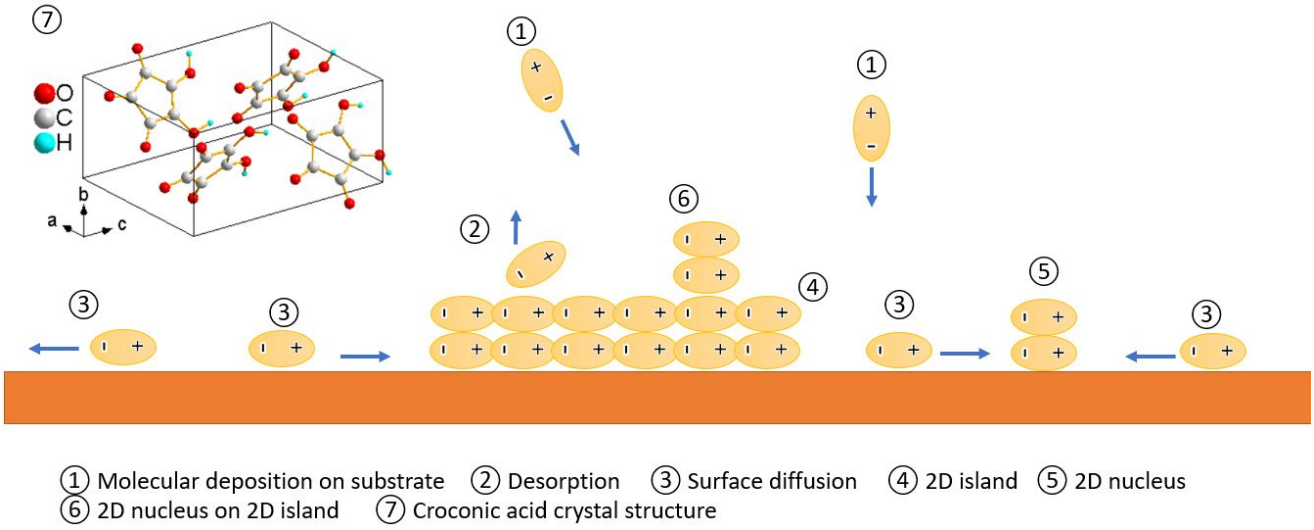

Fig. 1 Atomic model of CA molecular crystal and the film growth processes on a substrate where the CA molecules are represented by dipoles. The plus and minus signs represent the positive and negative poles of polar molecules respectively.

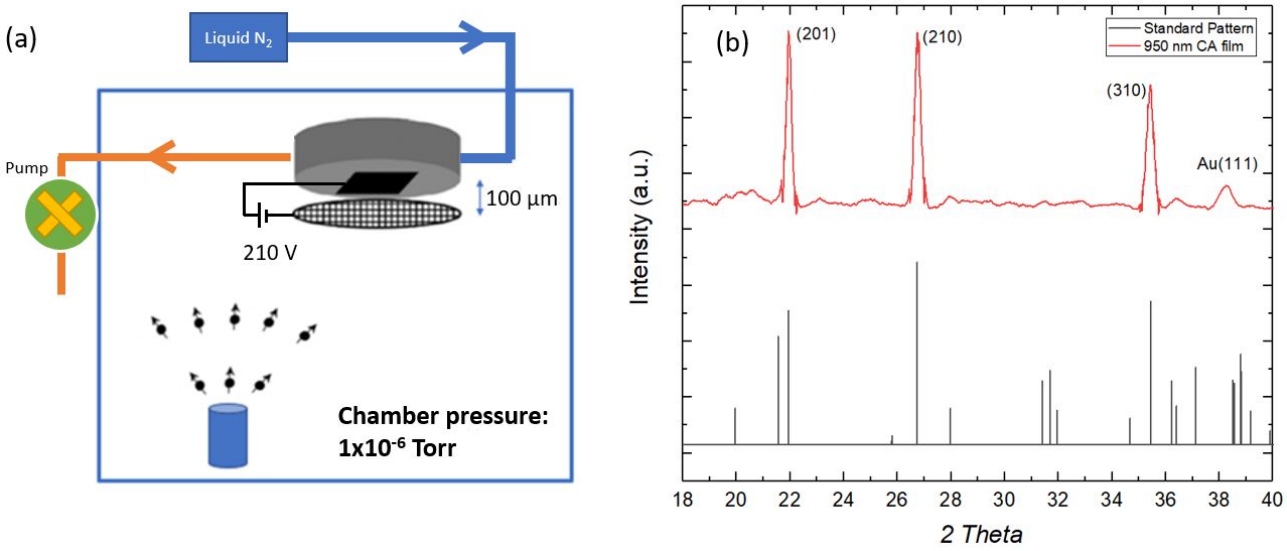

Fig. 2 (a) Experimental setup for the film growth under the electric field. (b) XRD patterns of the croconic acid films with the thickness of 950 nm, compared with the calculated patterns (see text).

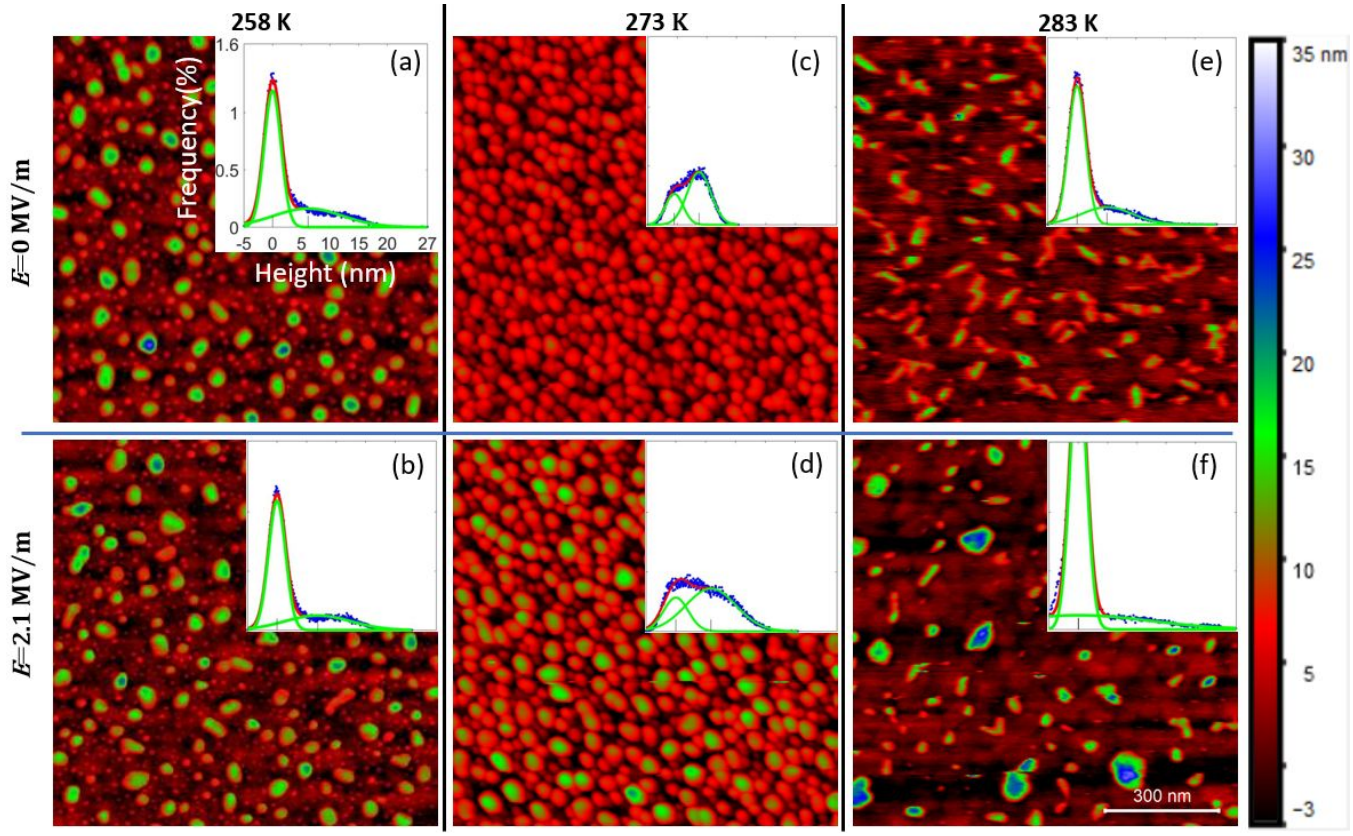

Fig. 3 AFM images of CA films grown with different substrate temperatures with and without the electric field under the same deposition time and distance. (a) and (b) 258 K; (c) and (d) 273 K; (e) and (f) 283 K and different electric field strength. The insets are corresponding height histograms whose horizontal and vertical axes are height and frequency respectively. Green lines are deconvoluted gaussian peaks whose peak positions are marked with short vertical lines on *x*-axes. All the images have the same scale bar as in (f).

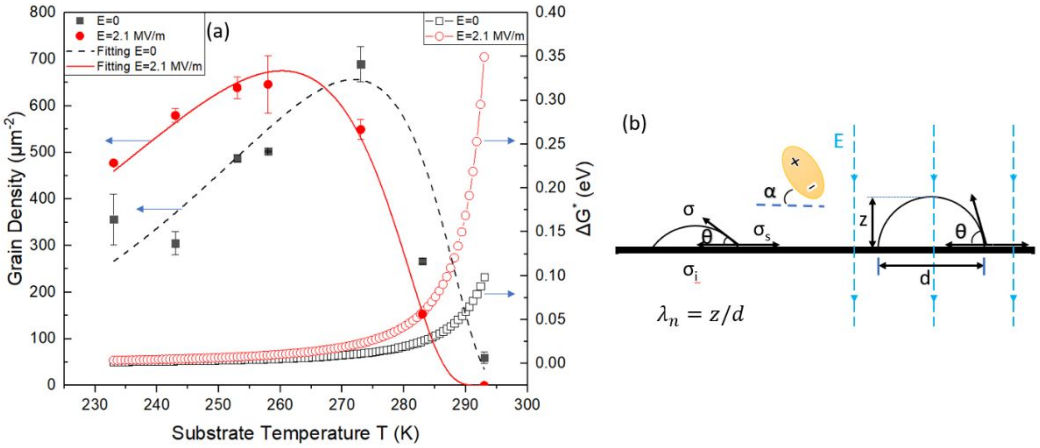

Fig. 4 (a) Grain density and nucleation barrier as a function of the substrate temperature with and without the electric field. (b) the diagram of heterogeneous nucleation process with and without the electric field.

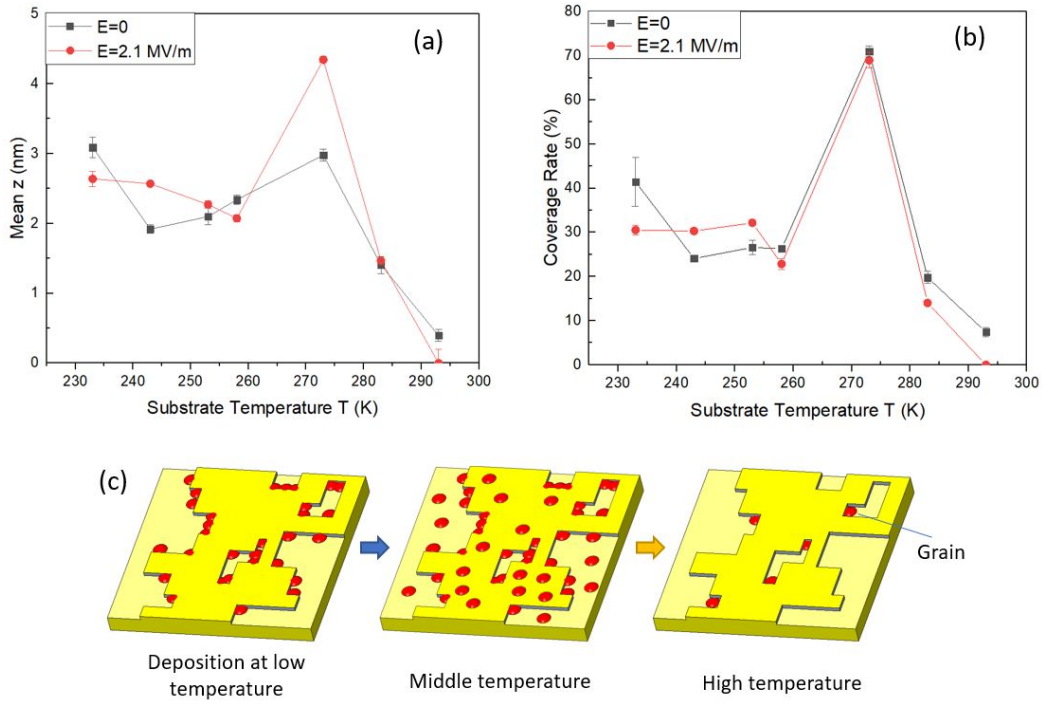

Fig. 5 (a) The average thickness and (b) the coverage rate of CA films versus substrate temperature with and without E. (c) The diagram of growth processes at different temperatures.

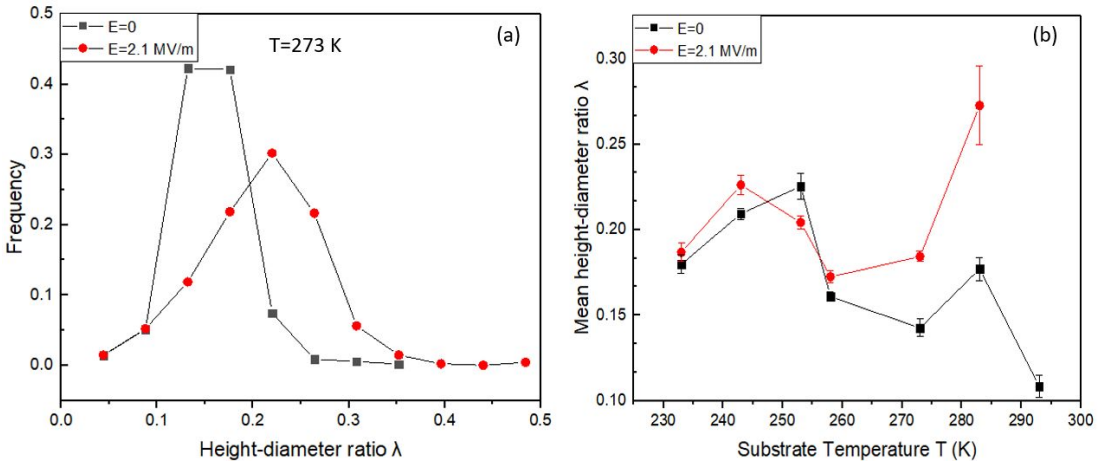

Fig. 6 (a) The normalized histogram of the height-diameter ratio for the CA film deposited at 273 K. (b) The mean height-diameter ratio versus substrate temperature with and without the electric field.

Table 1. Fitted parameters for the model function with and without the electric field.

E (MV/m)	Γ (×10^5)	E_{tr} (eV)	Ω (10^{-4} eV)	T_m (K)
0	4.7 ± 0.6	0.19 ± 0.01	1.2 ± 0.1	303.4 ± 0.2
2.1	0.8 ± 0.1	0.139 ± 0.003	1.9 ± 0.2	299.9 ± 0.9